PERGAMON

Aerosol Science 34 (2003) 1061–1084

Journal of
Aerosol Science

www.elsevier.com/locate/jaerosci

Polycyclic aromatic hydrocarbon size distributions in aerosols from appliances of residential wood combustion as determined by direct thermal desorption—GC/MS

Michael D. Hays[a,*], N. Dean Smith[a], John Kinsey[a], Yuanji Dong[b], Peter Kariher[b]

[a] *National Risk Management Research Laboratory, U.S. Environmental Protection Agency, 109 Alexander Dr MD, E343-02 Air Pollution, Prevention and Control Division, Research Triangle Park, NC 27711, USA*
[b] *ARCADIS, Research Triangle Park, NC 27713, USA*

Received 4 February 2003; received in revised form 7 April 2003; accepted 7 April 2003

Abstract

In this work, a direct thermal desorption/gas chromatography/mass spectrometry (TD/GC/MS) method is implemented to determine the polycyclic aromatic hydrocarbon (PAH) composition (MW = 202–302 amu) in size-segregated aerosols from residential wood combustion. Six combustion tests are performed with two commonly burned wood fuel species, Douglas-fir (*Pseudotsuga* sp.) and white oak (*Quercus* sp.). Atmospheric dilution and cooling of the aerosol plume are simulated in a newly designed wind tunnel, and the resulting aerosols are size classified with an electrical low-pressure impactor (ELPI). ELPI stage data speciated by TD/GC/MS were inverted and modeled using a log normal distribution function. Gravimetrically determined $PM_{2.5}$ (fine particles with aerodynamic diameters $[d_a] < 2.5$ μm) emission rates (2.3–10.2 g/kg) corroborate to matrix-corrected ELPI mass measurements of stages 1–8 (2.7–11.8 g/kg). Fuel moisture content linearly correlates ($r^2 = 0.986$) to the $PM_{2.5}$ mass geometric mean diameter (d_g). Combustion efficiency (CO_2/CO) and temperature, O_2 levels, and gas dilution temperature affect particle size distributions; d_g ranges from 313 to 662 nm, indicating an accumulation mode. Reconstruction and summation of inverted ELPI data allow for the quantification of 27 individual PAHs (and clusters of structural PAH isomers); PAHs characterize between 0.01 and 0.07 wt% of the $PM_{2.5}$ mass. Benzo[*a*]pyrene predominates the PAH emissions. PAH size allocations (d_g range = 171–331 nm) are out of phase with $PM_{2.5}$ mass ones and shifted to finer d_a. Higher and lower MW PAHs preferentially segregate to fine and coarse d_a in that order. The ultrafine mode contains on average greater than 80% of the total measured particle number concentration. Values of d_g for particulate matter surface area distributions are between 120 and 330 nm. For these tests, PAH mass and PM surface area linearly correlate ($r^2 \geqslant 0.913$). Application of a simple function to consider adsorption and absorption

* Corresponding author. Tel.: +1-919-5413984; fax: +1-919-5410359.
E-mail address: hays.michael@epa.gov (M.D. Hays).

0021-8502/03/$ - see front matter
doi:10.1016/S0021-8502(03)00080-6

mechanisms makes apparent that (a) surface and core compositions of PAH of identical MW groups vary with combustion and (b) preferential surface adsorption of lower MW PAH is possible.

Keywords: Thermal desorption; ELPI; PAH; Particulate matter

1. Introduction

Substantial evidence links respirable particulate matter (PM) to human morbidity and mortality, especially in susceptible subpopulations (Dockery et al., 1993; Pope, 2000; Samet, Dominici, Curriero, Coursac, & Zeger, 2000). Deposition efficiency of PM in respiratory tract zones (tracheobronchial, pulmonary, nasopharyngeal, and thoracic) of humans is size dependent (Phalen et al., 1991; Swift, 1995; Balashazy, Hofmann, & Heistracher, 1999); fine particles (aerodynamic diameter, d_a, <2.5 μm, $PM_{2.5}$) for example are primarily confined to the lower respiratory zones (Tsuda, Rogers, Hydon, & Butler, 2002). Discrete size classifications [coarse ($d_a < 10$ μm, PM_{10}), fine, and ultrafine ($d_a < 0.1$ μm)] of PM of urban air induce different biological toxicity in in vitro and in vivo models due in part to their chemical compositions varying by size (Diociaiuti et al., 2001; Hauser, Godleski, Hatch, & Christiani, 2001; Oberdörster, 2001). With several anthropogenic and biogenic source types contributing to the airborne fine PM mixture, comprehension of the chemical composition by size on a source category basis is essential from air quality modeling, regulatory, and health standpoints.

Aerosol time-of-flight-mass-spectrometry (ATOFMS) (Silva & Prather, 1997; Silva, Liu, Noble, & Prather, 1999), temperature-programmed thermal desorption particle beam mass spectrometry (TPTDP) (Tobias & Ziemann, 1999; Tobias et al., 2001) and off-line analysis of impactor collection substrates (Kleeman, Schauer, & Cass, 1999, 2000) are examples of approaches used to size segregate and chemically profile source emissions. On-line ATOFMS classifies in real time the inorganic and organic chemical species of individually sized particles but is limited to chemical species identification. From the standpoint of the organic chemical composition of nanoparticles within a defined size mode, TPTDP discriminates further than ATOFS but is only semi-quantitative to date. In comparison, impactor-based, off-line methods are quantitative and can be applied to determine organic and elemental carbon, trace element, and water-soluble ion (sulfate, nitrate, and ammonium) concentrations within impactor-resolved particle size fractions.

In airborne PM, size distributions of polycyclic aromatic hydrocarbons (PAHs) (see, for example, Allen et al., 1998 or Offenberg & Baker, 1999), some of which are employed as molecular markers for source apportionment, and oxygenated PAHs (Allen et al., 1997) were determined by impactor-based methods in past work. The thermal desorption/gas chromatography/mass spectrometry (TD/GC/MS) approach of Falkovich and Rudich (2001), in particular, overcomes many of the significant analytical challenges associated with the examination of organics in the airborne PM. Their method requires no sample preparation, small sample mass, is rapid, sensitive, and accurate and would, on a temporal basis, offer better resolution of episodic air pollution events. As efforts intensify to develop air quality models that consider size-based particle chemistry, the development of precise size-resolved source profiles is desirable. To the best of our knowledge, size distribution data of individual organic species from carbon-based emission sources using the thermal desorption (TD)

technique are virtually nonexistent. These data are needed to advance air quality model predictions of air parcels polluted with size-distributed chemical mixtures.

In this work, a direct (TD/GC/MS) method is utilized to determine the PAH composition in size-segregated PM from RWC, a major fine PM source. In the US alone, RWC emits PM to the atmosphere at a rate of 1.1×10^6 metric tons/yr, and up to 30% of the atmospheric PM flux in the winter months in certain regions can be attributed to RWC (Nolte, Schauer, Cass, & Simoneit, 2001). In emerging countries, it is a significant source of fine PM in poorly ventilated indoor air (Oanh, Nghiem, & Phyu, 2002). These particles by mass ($\approx 95\%$) have $d_a < 400$ nm, are rich in organic carbon ($> 70\%$), chemically complex, adversely impact health (Larson & Koenig, 1994; Pintos, Franco, Kowalski, Oliveira, & Curado, 1998) and are mutagenic (Oanh et al., 2002). Because this toxicity and the PAHs in PM may be linked (Schoey, 1998; Vinggaard, Hnida, & Larsen, 2000), we closely examine the size distribution of a wide molecular weight range (202–302 amu) of PAHs from RWC. Relative PAH concentrations can vary with combustion and wood fuel conditions; thus, wood combustion appliances, flame phases, and fuels of different moisture contents and species (*Quercus* sp. and *Pseudotsuga* sp.) were studied.

2. Experimental

2.1. Fuels

Two wood fuel species, Douglas-fir (*Pseudotsuga* sp.) and white oak (*Quercus* sp.), were selected for testing. These fuels ranked among the top 10 in a nationwide (United States) availability index for residential wood burning (Fine, Cass, & Simoneit, 2001). Fuel sources were collected from northern Durham County, NC (oak) and received from Myren Consulting of Colville, WA (Douglas-fir). Wet oak samples were gathered and split on the day of testing. Wet oak logs were stored (if necessary) in stacks outside, intact, and uncovered. Dry oak samples were split upon delivery and stored inside the woodstove laboratory. The Douglas-fir samples at two moisture levels were shipped in large wooden crates, where they remained until testing. On each fuel subsample, moisture contents (Table 1) were measured as received using ASTM methods D2961, D3302, D3173. Pre-burn fuel compositions with ASTM method D3176 were also obtained on each fuel subsample and showed virtually identical atomic mass wt/wt values. Found: C, 42.2–42.8; H, 6.6–6.8; N, < 0.5; O, 50.4–51.3; S, < 0.05; Cl, 20–33 ppm. All values are given as percentages unless noted otherwise.

2.2. Fuel combustion

Six combustion experiments were performed in a wood-fired test facility detailed by others (Purvis, McCrillis, & Kariher, 2000; Gullett, Touati, & Hays, 2003). The facility houses residential fireplace (MRC42A; Majestic, Ontario, Canada) and noncatalytic woodstove (3100; Quadrafire, Colville, WA) appliances, both of which were engaged here. The woodstove was freestanding, fabricated from steel and had a glass window in the front door. The zero-clearance fireplace contained a log grate and glass door. These units were typical of those currently available to consumers in US markets and tested in previous experimental programs, thereby providing a large body of data to which the current study can be compared. For this effort, experimental methods for wood combustion in these appliances

Table 1
Fuel test matrix, preburn fuel composition, and wind tunnel sampling parameters used for residential wood combustion experiments

	Wood fuel type					
	Quercus sp./Oak				*Pseudotsuga* sp./Douglas-fir	
	Fuel test matrix[a]					
Test identification	WSOH1	WSOH2	WSOL	FPOH	WSDL	WSDH
Appliance type	WS	WS	WS	FP	WS	WS
Fuel mass burned (kg)	14.8	14.7	14.6	20.5	14.4	14.9
Moisture content (%)	29.2	28.4	12.2	29.7	12.2	24.2
	Sampling parameters[b]					
Sampling time (min)	302	332	272	266	310	322
Fuel burn rate (kg/h)	2.9	2.7	3.1	4.6	2.8	2.8
Dilution ratio	547	493	843	32	780	618
Wind tunnel temp (°C)	13.5	13.0	9.4	21.0	5.1	16.8
Stack temp 1 (°C)	186.6	200.1	231.4	90.5	266.6	225.4
Stack temp 2 (°C)	130.5	137.5	153.0	87.0	172.6	151.6
Stack flow rate (m^3/min)	1.1	1.2	0.71	18.7	0.76	0.96
ELPI sampling rate (l/min)	9.6	9.6	9.6	9.6	9.6	9.6
Residence time (s)	6.5	6.5	6.5	6.5	6.5	6.5
	Emissions characterization[c]					
CO (ppm)	3203	2773	2730	325	3542	3771
CO_2 (%)	2.4	2.2	2.8	0.6	4.7	4.1
O_2 (%)	17.0	17.5	17.2	19.8	15.5	15.7
NO (ppm)	26.1	25.3	20.1	11.3	20.9	18.1
EC/OC (%)	2.0	1.0	1.7	6.7	4.3	2.7
$PM_{2.5}$ mass (g/kg)	8.8	10.2	4.9	8.6	2.3	6.3
Inverted ELPI mass stages 1–8	9.2	11.8	—	10.1	2.7	7.9
r^2	0.999	0.996	—	0.726	0.935	0.967
PM mass d_g (nm)	662	662	—	320	313	530

[a]Appliance type, WS—Quadrafire 3100 woodstove and FP-Majestic (MRC42a) fireplace; fuel mass burned was continuously measured using a platform balance (Model 2185; Toledo Scale); fuel moisture contents were measured as received using ASTM methods D2961, D3302, and D3173.

[b]$CO_{stack}/CO_{dilution}$ was used to determine dilution ratio; wind tunnel temp, tests were performed in months typical for RWC operation (March and April); Stack temp 1-obtained 0.15 m from the RWC appliance; Stack temp 2-obtained 2.4 m from the RWC appliance at the continuous emissions monitor intake (Type K thermocouples); Wind tunnel flow rate was calculated using both CO tracer gas measurements and a multimeter (Shortridge Instruments, Inc., Scottsdale, AZ).

[c]CO, CO_2, NO, and O_2 represent an average of measurements over the total sampling period; $PM_{2.5}$ Mass, gravimetrically measured and expressed in units of grams of PM per kilograms of dry biomass burned; For WSOL, ELPI data failed to fit to the lognormal distribution function; r^2 is a measure of the ability of the log normal distribution function to fit ELPI test data.

complied with U.S. EPA (U.S. EPA, 2001) certification standards and were identical to those already described (Gullett et al., 2003). Test controls were in place for fire ignition, fuel load configuration, supplementary fuel charging, operational cycles, burn rates, air delivery and circulation patterns,

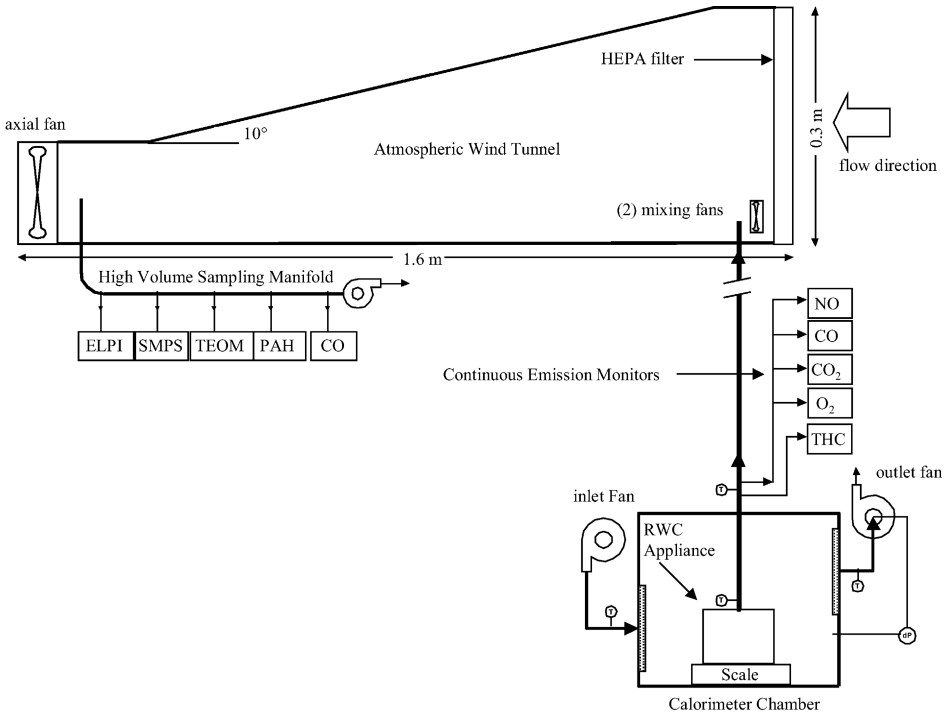

Fig. 1. Schematic diagram of experimental design for wood combustion testing and sampling using the wood stove appliance and wind tunnel dilution.

and to some extent, combustion phase (kindling/high/low). Each test was assigned identification indicating fire appliance (WS-woodstove or FP-fireplace), fuel species (O-oak or D-Douglas-fir), and fuel moisture content level (H-high [> 24%] or L-low [13%]) (see Table 1). Duplicate burns were performed in the woodstove with an oak wood that contained high moisture (> 28%). They were designated WSOH1 and WSOH2.

2.3. Sampling of combustion emissions

To adequately sample and mimic atmospheric dilution and cooling of the aerosol plume, a newly designed atmospheric wind tunnel fabricated from stainless steel was utilized (Fig. 1). Briefly, stack emissions were directed from the RWC appliance to mixing fans positioned at the wind tunnel entrance. Perpendicular to the stack emissions, HEPA-filtered dilution air was introduced. Just prior to exiting the tunnel through an axial fan, a diluted ($\sim 600 : 1$ at $\sim 7.2°C$) aerosol sample was extracted with a high-volume sampling manifold. At this test section, temperature, relative humidity, and CO emissions (Rosemount 880) were measured. Also positioned at this wind tunnel section and of significance to this work was the electrical low-pressure impactor [(ELPI) Model 97 2E; Dekati Ltd., Finland], which collected and classified particles by size, number, and mass. CO_2 (Rosemount 880), NO (Teco Model 10), total hydrocarbon [(THC) Teco Model 51], and O_2 (Rosemount 755) emissions and temperature measurements of the combustion reaction were taken at the stack

(2.4 m height) of the RWC appliance. Temperature measurements were also taken closer to the combustion zone (0.15 m height). A gravimetric determination of $PM_{2.5}$ mass was achieved at this section with a Teflon filter (Pall Gelman) placed downstream of a $PM_{2.5}$ cyclone. Table 1 and its footnotes provide a fuel test matrix and supplemental experimental details for all of the associated sampling measurements.

Ancillary test equipment was also used to sample RWC emissions and shown in Fig. 1. Data from these instruments are forthcoming, will be used to further support physical and chemical characterization studies of particulate matter, and for an inter-comparison study among (ELPI) instrument sets.

2.4. Electrical low pressure impactor

Aerosols were classified by size interval (d_a) with an ELPI sampling at a rate of 9.1 l/min (Keskinen, Pietarinen, & Lehtimaki, 1992). The ELPI flow was calibrated (Gilibrator; Sensidyne, Clearwater, FL). The cut diameters (size of particles collected with 50% efficiency) of stages 1–13 were 0.03, 0.061, 0.11, 0.17, 0.27, 0.40, 0.65, 1.00, 1.63, 2.48, 4.02, 6.76, and 10.26 μm, respectively. Our focus was on the lower ELPI stages 1–8 because they characterized particle size distributions in the range of 0.01–2.9 μm; wood combustion PM typically is within this range (Kleeman et al., 1999; Purvis et al., 2000). Precisely punched (26 mm diameter), smooth aluminum foil substrates were placed over the impaction plates for collection of particulate mass. Prior to testing, the collection substrates were rinsed with acetone and dried at room temperature ($\sim 20°C$). Analysis of substrate blanks revealed no PAH compounds. To limit chemical interferences and to keep gas-phase semivolatiles from partitioning into grease, the coating of collection substrates with grease to reduce sampling bias from particle bounce was not practiced. The semisolid nature of wood smoke particles (condensable organic droplets) was expected to adequately limit particle bounce. Throughout testing, aerosol temperature (Table 1) and instrumental operating conditions were checked and within the manufacturer-specified ranges. After a combustion experiment, the ELPI was disassembled, and the sample collection substrates were removed, placed in plastic petri dishes, conditioned in a control chamber (24 h, 20–25°C, and 30–40% RH), and stored in a cryofreezer ($-50°C$) until analysis. In between combustion experiments, the impactor and particle charger (unipolar positive polarity) were solvent cleaned, calibrated, and then zeroed.

2.5. Chemical composition by direct TD/GC/MS

To determine the chemical composition of the size-classified particulate matter on the ELPI collection substrates, a TD/GC/MS analysis was performed. Prior work with standard reference material (SRM 1649a—National Institute of Standards and Technology [NIST]) assured the applicability of the TD technique for analysis of PAHs in PM (Waterman, Horsfield, Leistner, Hall, & Smith, 2000; Falkovich & Rudich, 2001). Adequate linearity ($r^2 \geqslant 0.971$), accuracy (quantified values overlap [95% confidence] the NIST-certified values), and method precisions (7–33% RSD) were reported. Experiments with SRM 1649a completed with our TD equipment indicated similar method precisions ($N = 3$; 6–32% RSD), high retention time reproducibility (Table 1), and adequate agreement to the certified NIST values (fail to reject 10 of 20 PAHs at 95% confidence; all within 25%).

A single combustion test comprised a set of 8 ELPI substrates, characterizing stages 1–8. Prior to the analysis, each individual ELPI collection substrate was thawed in a laminar flow clean hood (~10 min), placed in a pre-conditioned (350°C, 12 h) glass desorption tube (178 mm long; 6.0 mm outside diameter), and spiked with a deuterated internal standard suite. PAHs were not detected in the empty, pre-conditioned TD tubes. The preparation, certification, and chemical composition of the suite were previously described (Hays, Geron, Linna, Smith, & Schauer, 2002). Once spiked, the glass tube and sample were immediately inserted into a TD system [TDS2; Gerstel Inc., Baltimore, MD] directly interfaced to a GC/MS [Model 6890/5973; Hewlett Packard; Pal Alto, CA]. The thermal extraction was achieved by ramping the TDS2 oven temperature from 25°C to 300°C at 12°C/min; pyrolytic degradation of organic compounds was minimized by avoiding temperatures greater than 300°C. The small sample size (the sample mass range = 7–283 μg of PM) allowed for improved resolution and ensured that the column capacity was not exceeded. Helium (20 ml/min) was passed over the sample throughout desorption, which was performed in splitless mode. This step augmented analyte removal from the semisolid particle matrix. The TDS2 model has an adjustable He flow feature. As evidenced by additional experiments, extraction efficiencies did not increase with He flow rates greater than 20 ml/min. Desorbed analytes passed through a short (152 mm), heated (300°C) inert steel (SilcoSteel) transfer line and were then trapped on a cryogenically cooled (−100°C, liquid N_2) programmable temperature (PTV) inlet system (CIS), also operating in splitless mode. The inlet liner was packed with a glass wool solid support, which enhanced the cryofocussing of the analytes and trapped unwanted materials.

Upon completion of the desorption step, the TDS2 oven was rapidly cooled with cryofluid to ambient temperature (25°C). The CIS was then ballistically heated (720°C/min) to 300°C, which transferred the analytes in plug form to an ultra-low bleed GC capillary column (5% diphenyl-95% dimethyl siloxane copolymer stationary phase [30-m length; 0.25 μm film thickness; 0.25 mm i.d.]). The GC oven temperature was held at 65°C for 10 min, ramped at 10°C/min to 300°C, and then held constant for 41.5 min. The MS detector was operated in scan mode (50–500 amu, 3 scans/s). Enhanced Chemstation (V. B.01.00, Hewlett Packard) software was used to control the GC/MS and CIS and for data acquisition. Gerstel MASter (Version 1.76 × 5) software was used to monitor and control the TDS2 operation.

Upon the completion of a run, a routine carryover test was performed by a subsequent TD/GC/MS analysis of the spent sample. There was no carryover of PAHs. However, slight carryover of highly polar organics of the methoxyphenol class was detected, particularly at high particulate mass loadings. Concentrations of methoxyphenols, which function as molecular markers of wood smoke, in the carryover were typically less than 20% wt/wt of those determined by the original extraction. The polar residue was experimentally isolated within the TDS2 system along the flow path to and in the locking cone and was not due to an incomplete extraction. Mild sonication in hexanes and methanol and baking (300°C ⩾ 1 h) cleaned the affected TDS2 components as needed. Since the TD method is sensitive for methoxyphenols, we are evaluating its potential application to samples with a lower particulate mass.

Quantification of PAH was accomplished with a calibration database of response ratios formed from certified authentic and isotopically labeled internal standard suites. Listed in Table 2 are the specific PAH targets, their calibration range, r^2 for three levels, molecular mass and formula values, and retention time reproducibility values. Identification of sample analytes was categorized as positive if their retention time and mass spectrum were identical to that of the authentic or library standards.

Table 2
GC/MS calibration data for PAH and oxy-PAH compounds

Compound	Calibration range[a] TD (ng)	r^2 TD	Molecular weight (amu)	Molecular formula	RT RSD[b] (%)
PAH					
Fluoranthene	0.80–3.8	0.999	202	$C_{16}H_{10}$	0.00
Pyrene	0.40–1.9	0.999	202	$C_{16}H_{10}$	0.00
Acepyrene	0.50–2.0	0.980	226	$C_{18}H_{10}$	
Methylchrysene	0.10–0.40	0.986	242	$C_{19}H_{14}$	
Chrysene and triphenylene	0.40–1.9	1.000	228	$C_{18}H_{12}$	0.00
Benzo[*a*]anthracene	0.40–1.9	1.000	228	$C_{18}H_{12}$	0.17
Benzo[*k*]fluoranthene	0.40–1.9	0.961	252	$C_{20}H_{12}$	0.00
Benzo[$b + j$]fluoranthene	0.80–3.8	0.997	252	$C_{20}H_{12}$	0.02
Benzo[*a*]pyrene	0.40–1.9	1.000	252	$C_{20}H_{12}$	0.02
Benzo[*e*]pyrene			252	$C_{20}H_{12}$	
Benzo[*a*]fluoranthene			252	$C_{20}H_{12}$	
Perylene			252	$C_{20}H_{12}$	
Indeno[1, 2, 3-*cd*]pyrene	0.40–1.9	0.991	276	$C_{22}H_{12}$	0.03
Dibenzo[*ah*]anthracene	0.80–3.8	0.999	278	$C_{22}H_{14}$	0.03
Benzo[*ghi*]perylene	0.80–3.8	0.983	276	$C_{22}H_{12}$	0.02
Anthanthrene			276	$C_{22}H_{12}$	
Dibenzo[*aj*]anthracene			278	$C_{22}H_{14}$	
Pentaphene			278	$C_{22}H_{14}$	
Benzo[*b*]chrysene			278	$C_{22}H_{14}$	
Coronene	0.50–2.4	0.964	300	$C_{24}H_{12}$	0.02

[a]Calibrated with a minimum of three calibration levels; acepyrene calibrated using single-point (1.96 ng/μL); benzo[*e*]pyrene, benzo[*a*]fluoranthene, and perylene quantified with benzo[*a*]pyrene response; anthanthrene quantified with benzo[*g*, *h*, *i*]perylene; dibenzo[*a*, *j*]anthracene, pentaphene, and benzo[*b*]chrysene quantified with dibenzo[*ah*]anthracene response; benzo[*j*]fluoranthene coelutes with benzo[*b*]fluoranthene and dibenzo[*ah*]anthracene coelutes with dibenzo[*ac*]anthracene.

[b]Retention time relative standard deviation-calculated from replicate ($N = 3$) TD/GC/MS analyses with NIST SRM 1649a. Additional notes: Dibenz[*ah*]anthracene-d14 and chrysene-d12 were used as internal standards.

The relative retention times of Wise, Sander, Schantz, Hays, and Benner (2000) and the NIST mass spectral library identified PAH compounds for which an authentic standard was unavailable. These compounds were quantified using the responses of a structural isomer. GC/MS calibration data were verified on a daily (24 h) basis using an authentic standard suite. If 75% of the organic compounds checked were within 20% of their certified values the calibration was accepted, if not recalibration and GC/MS maintenance (if necessary) were performed.

3. Inversion of ELPI–TD/GC/MS data

Particle loss in the ELPI due to an increased trap voltage at the corona needle can be high compared with the minor post-charger losses ($< 2\%$ above 30 nm) from diffusion, interstage, space charge, and image charge effects (Marjamaki, Keskinen, Chen, & Pui, 2000; Virtanen, Marjamaki,

Ristimaki, & Keskinen, 2001). With this work developed as part of a broader research effort, the ELPI particle charger voltage was activated so that electrical detection and continuous, real-time (5 s resolution) measurements were realized. With chemical analysis executed subsequent to the ELPI measurements, accounting for the charger efficiency was required and achieved with a theoretical penetration curve provided by the ELPI manufacturer. An independent verification of the manufacturer specifications was achieved over the size range of interest (Marjamaki et al., 2000). For each size bin, mass compensation (ng/m^3) for each analyte quantified by TD/GC/MS was accomplished.

Fixed internal mixing (i.e., chemical composition) of the source aerosol within a given size mode was assumed. This assumption of homogeneity in ELPI-defined size modes for PAH in aerosols was likely satisfied for the controlled biomass combustion tests performed here although its extension to ambient air parcels of mixed sources may prove difficult due to their nonuniform chemical composition by size. Individual or groups of particles within an ELPI-defined size mode having unique chemical and/or physical attributes that allow for their selective removal by any loss mechanism may upset this assumption of homogeneity. Not yet considered for this source are the compositional (e.g., ionic, organic and elemental carbon) and physical (e.g., aspect ratio and morphology) differences among particles within the same ELPI-defined size mode, nor is their effect on loss mechanisms due to charging. Moreover, the degree to which particles are preferentially lost or misclassified due to nonideal aerodynamic behavior is unclear but could also complicate this assumption of homogeneity.

ELPI stage data are not actual size distributions. Thus, to obtain independent instrumental size distributions, TD/GC/MS data (for stages 1–8) were inverted. Data inversion sharpens size resolution and is achieved using kernel functions that define ELPI size cutoff properties. It also allows for comparisons of size distributions of the individual organic species across different impactor types and is performed here for each PAH species by assuming a continuous lognormal particle size distribution. Eq. (1) gives the lognormal distribution function.

$$\frac{\mathrm{d}m}{\mathrm{d}\log d_a} = \frac{m}{\log \sigma_g \sqrt{2\pi}} \exp\left[\frac{-(\log d_a - \log d_g)^2}{2\log^2 \sigma_g}\right]. \tag{1}$$

Three fitting parameters (m, the total compound mass across all particle size bins; d_g, the geometric mean diameter; σ_g, the geometric standard deviation) determine the distribution shape and position.

The inversion algorithm required knowledge of the stage collection efficiencies as a function of particle size. With monodisperse aerosols, experimental collection efficiencies of different ELPI stages (E_i) were calibrated (Marjamaki et al., 2000). These calibration data were applied here, presuming that the impactors of both studies had identical geometry and were operated under similar conditions. To approximate the sigmoidally shaped collection efficiency curves, the expression of Winklmayr, Wang, and John (1990) was used (Eq. (2)):

$$E_i(d_a) = \left[1 + \left(\frac{(d_{50})_i}{d_a}\right)^{2S_i}\right]^{-1}, \tag{2}$$

where [$(d_{50})_i$, the cutoff diameter of the ith stage ($i = 1, 2, \ldots, N$); S_i, the steepness of the ith stage]. Cutoff diameter is defined as the diameter of a spherical particle of unit density that is collected with 50% efficiency and determined gravimetrically. Greater steepness (S_i) is preferred to increase

sensitivity between impactor stages and solved using Eq. (2) and the data of Marjamaki et al., (2000).

A series of kernel functions (k_i) were then derived from stage collection efficiencies, as shown in Eqs. (3) and (4).

$$k_N(d_a) = E_N(d_a) \quad \text{for } i = N, \tag{3}$$

$$k_i(d_a) = E_i(d_a)[1 - E_{i+1}(d_a)] \cdots [1 - E_N(d_a)] \quad \text{for } i = 1 \text{ to } N - 1. \tag{4}$$

With N as the number of stages; impactor stage 1 collects the smallest particle diameters.

Eq. (5) relates the compound mass collected on the ith stage of the ELPI to the log normal distribution

$$m_i = \int k_i(d_a)\, Pe(d_a)\, \frac{m}{\log \sigma_g \sqrt{2\pi}} \exp\left[\frac{-(\log d_a - \log d_g)^2}{2 \log^2 \sigma_g}\right] \mathrm{d} \log d_a \tag{5}$$

$Pe(d_a)$ is the fraction of particles with a d_a that penetrates the ELPI charger. The theoretical penetration curve correlates well ($r^2 = 0.999$) to a polynomial fit, Eq. (6).

$$Pe(d_a) = -1.2431 + 1.41274 \log(d_a) - 0.2623(\log(d_a))^2. \tag{6}$$

Eq. (5) can be expressed as a summation

$$m_i = \sum_{j=1}^{P} k_{i,j}\, Pe_j\, \frac{m}{\log \sigma_g \sqrt{2\pi}} \exp\left[\frac{-(\log d_j - \log d_g)^2}{2 \log^2 \sigma_g}\right] \delta \log d_j, \tag{7}$$

where m_i is the mass of compound on stage i; d_j is the particle diameter at the jth point; the number of points (P) over which the size distribution is evaluated is 200, and $k_{i,j} = k_i(d_j)$.

A set of N equations (Eq. (7)) relates the particle size distribution to the compound mass on each stage. Using the Marquardt method, the equation set was solved numerically for m, d_g, and σ_g. The values of m, d_g, and σ_g are chosen so as to minimize the sum of the squares of the differences between the analytically determined compound mass values and those predicted by the model. TD/GC/MS was used to quantify the compound mass as it corresponds to the several different ELPI stages. The correlation coefficient (r^2) is calculated with Eq. (8) and measures the degree to which these mass values are linearly related.

$$r^2 = \frac{\sum_{i=1}^{N} (m_i - m_a)(mc_i - mc_a)/(N-1)}{\sqrt{\sum_{i=1}^{N} (m_i - m_a)^2/(N-1)} \times \sqrt{\sum_{i=1}^{N} (mc_i - mc_a)^2/(N-1)}} \tag{8}$$

where $m_a = \sum_{i=1}^{N} m_i/N$, $mc_a = \sum_{i=1}^{N} mc_i/N$, and mc_i is the inverted species mass for stage i.

Inversions were performed with in-house programs developed in Mathcad (Version 7; Mathsoft Inc. Cambridge, MA). From the above-estimated parameters, $\mathrm{d}M/\mathrm{d} \log d_a$ for each species was calculated and converted to the emission factor for that species.

4. Results and discussion

4.1. Gravimetric $PM_{2.5}$ mass emission rates

Gravimetrically determined mass emission factors of $PM_{2.5}$ for the RWC tests range from 2.3 to 10.2 g/kg (Table 1). For combustion in the woodstove appliance, the average mass emission factor and standard deviation of Douglas-fir and oak wood fuels are 6.5 ± 3.1 g/kg. In close agreement, woodstove combustion of a California oak shows $PM_{2.5}$ mass $= 7.1 \pm 1.6$ g/kg (Gullett et al., 2003). For the gravimetric data set, $PM_{2.5}$ mass emissions linearly correlate ($r^2 = 0.836$) to the fuel moisture content. Woodstove combustion experiments of others (McDonald et al., 2000) that use drier (moisture content $= 10.4 \pm 3.9\%$) mixed hardwood fuels also show lower $PM_{2.5}$ mass values (4.4 ± 2.0 g/kg). Uncertainty in combustion makes acquiring precise mass emission factors for RWC difficult. However, this study achieves high precision (10.4% RSD) for duplicate tests, WSOH1 and 2. This result is typical of the wood stove test facility used for this work (Gullett et al., 2003). For fireplace combustion of oak, a single test shows that $PM_{2.5}$ mass $= 8.6$ g/kg. Among the current fireplace emission studies completed using oak wood, $PM_{2.5}$ mass values of 5.7 ± 0.6 (Fine et al., 2001), 6.1 ± 1.5 (McDonald et al., 2000), 5.1 ± 0.5 (Schauer, Kleeman, Cass, & Simoneit, 2001), 6.2 (Rogge, Hildemann, Mazurek, & Cass, 1998) and 3.9 ± 0.4 g/kg (Gullett et al., 2003) are reported.

4.2. ELPI measured $PM_{2.5}$ mass

ELPI measurements of stages 1–8 are matrix corrected and inverted to produce emission factors of 9.2, 11.8, 10.1, 2.7, and 7.9 g/kg for tests WSOH1, WSOH2, FPOH, WSDL, and WSDH, respectively. These factors on average are within 86% (80–96%) of the gravimetrically determined $PM_{2.5}$ emissions. On average, stages 1–8 describe $> 90\%$ of the total inverted mass. The effect of particle density on stage mass response would explain why the mass values determined by ELPI are systematically higher than those obtained gravimetrically. Review of curves of ELPI channel multipliers versus particle densities indicates that the actual density of particles from wood combustion is higher than the assumed value of unity (Moisio et al. 1997).

For five of the six RWC tests, the ELPI data fit to a lognormal distribution function, giving an r^2 range of 0.726–0.999 (Table 1). The unimodal size distributions of $PM_{2.5}$ mass for these tests indicate an accumulation mode (Fig. 2). Test values of d_g range from 313 to 662 nm (Table 1), with the largest fraction of $PM_{2.5}$ in the submicron size mode. This result is characteristic of biofuel combustion (Kleeman et al., 1999; Purvis et al., 2000; Venkataraman & Rao, 2001). For all tests, a visual inspection of the upper 5 stages (9–13) confirms no particle mass deposits, precluding their analysis. Although coarse particle emissions ($d_a \geqslant 2.5$ μm) due to ejection of partially burned biomass, raw fuel, ash, or stack deposits might be evident at times because upstream of the ELPI sampler is devoid of a $PM_{2.5}$ cyclone. The ELPI collection substrates at the upper stages are uncoated. Due to impact with the upper stages, smaller fragments of coarse particles may form and carry over to lower stages, potentially distorting results. ELPI measurements for WSOL in particular show consistently increasing $dM/d\log d_a$ values over the size range (stages) of interest (see the Fig. 1 panel inlay to view a plot of the WSOL raw stage data). This pattern causes the inversion to fail due to the inability of the lognormal distribution function to fit the ELPI mass data. Particle bounce may also possibly explain what occurred over the WSOL test (McDonald, Zielinska, Sagebiel, & McDaniel,

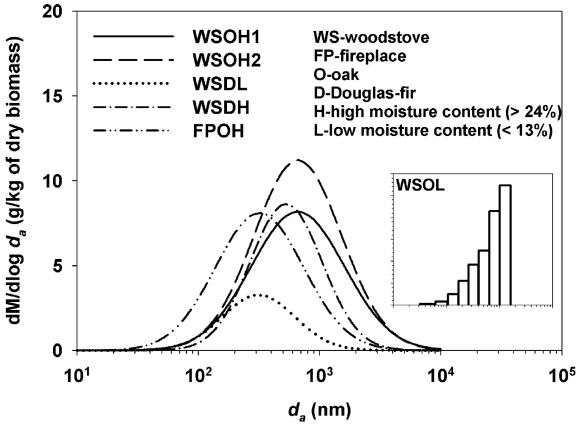

Fig. 2. Size distributions of $PM_{2.5}$ mass emissions from RWC as measured by ELPI.

2002). Regardless, this occurrence is atypical and unsupported by sampling and combustion parameter values for woodstove tests.

Among other variables, experimental dilution and cooling, sampling, fuel, and combustion conditions influence $PM_{2.5}$ mass distributions (Purvis et al., 2000). Briefly, for woodstove tests WSOH1 and 2, WSDL, and WSDH, moisture content linearly correlates ($r^2 = 0.986$) to the $PM_{2.5}$ mass d_g. FPOH (320 nm) and WSDL (313 nm) show the lowest d_g values. Purvis et al. (2000) suggest that combustion efficiency (as indicated by the test-averaged CO_2/CO ratio) to some extent controls mass emissions by particle size. In agreement, FPOH and WSDL also show the highest mean combustion efficiencies. For WSDL, the combustibility of dry Douglas-fir is evidenced by the higher stack temperature (266°C) and lower $PM_{2.5}$ emissions (2.6 g/kg). Relative to WSDL, FPOH shows higher (a) O_2 levels (19.8%) for combustion and (b) dilution temperature (21°C) in the wind tunnel for the air/aerosol mixture. Gas dilution temperature also affects particle size distributions (Purvis et al., 2000). Higher temperatures likely limit particle-phase partitioning of the organics, lessen agglomeration, and shift the mass distributions to smaller diameters. The high $[O_2]_g$ can help to encourage and sustain an intense flaming condition, which in turn produces a large mass concentration of smaller diameter particles.

4.3. Particle-phase PAH emissions

Total particle-phase emissions of 24 individual PAHs (and clusters of structural PAH isomers—see Table 3 footnotes) expressed in units of milligram per kilogram of dry biomass are given in Table 3. Reconstruction and summation of inversion data of ELPI stages 1–8 yield these values. Total quantified PAHs characterize between 0.01 (WSOL) and 0.07 wt% (WSDL) of the $PM_{2.5}$ mass. On a wt% basis, FPOH, WSDL, and WSDH (woodstove fires with *Pseudotsuga* sp.) show the highest PAH emissions. Elemental carbon/organic carbon (EC/OC) ratios in particulate were determined by OC/EC analysis (NIOSH Method 5040; thermal-optical transmittance) of quartz filters. For FPOH, WSDL, and WSDH, EC/OC ratios (Table 1) are comparably high, subtly associating PAH growth with EC formation. In rich combustion, polymerization reactions of 2- and 3-ring monomeric PAHs

Table 3
Total particle-phase PAH emissions (mg/kg of dry biomass burned) determined by inverting TD–GC/MS data of ELPI stages 1–8

Compounds	Wood fuel type (mg/kg of dry biomass burned)					
	Quercus sp./Oak				*Pseudotsuga* sp./Douglas-fir	
	WSOH1	WSOH2	WSOL	FPOH	WSDL	WSDH
Fluoranthene	0.1376	0.2566	*	0.0703	0.0501	0.1070
Pyrene	0.1256	0.2081	*	0.0730	0.0469	0.0901
Acepyrene	1.0041	0.6253	*	3.1388	0.8792	*
Methylchrysene	ND	ND	ND	ND	0.0292	*
Chrysene and Triphenylene	0.1684	0.1211	*	0.3167	0.0973	0.4754
Benzo[*a*]anthracene	0.1824	0.1039	*	0.4054	0.1046	0.6463
Benzo[*k*]fluoranthene	0.2466	0.2761	0.0634	0.3579	0.0909	0.4929
Benzo[$b+j$]fluoranthene	0.4488	0.3273	0.0816	0.3611	0.0909	0.4650
Benzo[*a*]pyrene	0.5575	0.5770	0.1147	0.6512	0.1635	0.8743
Benzo[*e*]pyrene	0.2867	0.4342	0.0961	0.3735	0.1027	0.4748
Benzo[*a*]fluoranthene	0.1867	0.1272	0.0348	0.2108	0.0468	0.3566
Perylene	0.0927	0.0848	0.0222	0.1071	0.0238	0.1351
Indeno[$1,2,3-cd$]pyrene	0.1856	0.0902	0.0671	0.3570	0.0895	0.4359
Dibenzo[$ah+ac$]anthracene	*	0.0067	0.0083	0.0290	0.0082	0.0457
Benzo[*ghi*]perylene	0.0918	0.0508	0.0375	0.1786	0.0457	0.1992
Anthanthrene	0.0245	0.0143	0.0122	0.0744	0.0107	0.0701
Total PAH MW 276	0.1688	0.1264	0.0760	0.1822	0.0504	0.2004
Dibenzo[*aj*]anthracene	0.0128	0.0109	0.0089	0.0391	0.0106	0.0500
Pentaphene	ND	ND	0.0019	0.0105	0.0013	0.0168
Benzo[*b*]chrysene	0.0063	0.0049	0.0032	0.0252	0.0057	0.0449
Picene	0.0072	0.0072	0.0041	0.0335	0.0071	0.0490
Coronene	0.0370	0.0100	0.0168	0.0731	0.0202	0.0945
Total PAH MW 300	0.0417	0.0151	0.0014	0.0376	0.0048	0.0565
Total PAH MW 302	0.0578	0.0428	0.0009	0.0295	0.0026	0.0548
Total PAH	4.071	3.523	0.651	7.136	1.983	5.435

ND-not detected; *-detected but data inversion failed; Total PAH MW 276, 300, 302-quantified with benzo[ghi]perylene (276) and coronene (300 and 302) and comprise clusters of six, five, and four resolved peaks that elute within 0.7, 1.3, and 1 min of one another, respectively, see www.nist.gov (Sanders & Wise) for possible structures and tenative identification of molecular isomers; Total PAH calculated by reconstructing inversion data of stages 1–8 and summing across individual compounds.

control formation of higher molecular weight PAH and soot (Violi, D'Anna, & D'Alessio, 1999). Clearly, the test-averaged combustion efficiency conceals transient fire events or the extent of a smoldering phase, which would likely further explain the elevated EC levels.

From two recently performed studies of hardwood combustion in woodstoves (McDonald et al., 2000; Gullett et al., 2003), a subset of 16 PAH concentrations from test averages ($N \geqslant 3$) is used for comparison purposes. The subset includes fluoranthene, pyrene, chrysene/triphenylene, benzo[$b+j+k$]fluoranthene, benzo[$a+e$]pyrene, perylene, indeno[$1,2,3$-cd]pyrene, benzo[*ghi*]perylene, anthanthrene, dibenz[$ah+ac$]anthrene, and coronene. To determine mass emissions of each PAH, McDonald et al. (2000) and Gullett et al. (2003) solvent extract $PM_{2.5}$ collected on quartz fiber

filters prior to GC/MS analysis. Among studies, robust comparisons between analytical methods for PAH are expected because the TD performance is verified with SRM1649a (Waterman et al., 2000), a material certified largely by solvent extraction/GC/MS.

The moisture contents and fuel type of WSOH1 and 2 best match those used by Gullett et al. (2003). Therefore, their mass emission factors are used for comparisons. For particle-phase PAHs with MW $\geqslant$ 252, emission factors of the studies agree to within 71% on average. Although some variation in emissions between the studies is noted; for example Gullett et al. (2003) show an enrichment (by $\sim$3 fold) of PAHs with MW $\geqslant$ 278 in $PM_{2.5}$. Their combustion efficiencies and $[O_2]_g$ are generally higher. Perhaps, the ELPI charging process partly destroys or converts these PAHs. Regardless, as with all of the studies being evaluated, the relative PAH distributions (across this MW range) are strikingly similar. McDonald et al. (2000) composite 8 woodstove combustion profiles of mixed relatively dry (9–15% moisture content) hardwood species. In comparison with this effort, our PAH emissions from combustion tests with drier fuels (WSOL and WSDL) are higher by roughly two-fold. However, normalizing these emissions to $PM_{2.5}$ mass shows these studies agree to within 93% on average for the PAH group (MW $\geqslant$ 252), noting that an aggregate concentration for benzo[$b+k+f$]fluoranthene is used.

Typically, particle-phase concentrations of lower molecular weight (202 $\leqslant$ MW $\leqslant$ 228) PAHs predominate wood smoke profiles regardless of appliance design, fuel class, or combustion environment (see, for example, Rogge et al., 1998 or Venkataraman, Negi, Sardar, & Rastogi, 2002). For the six source tests, we show in Fig. 3 relative PAH distributions that contrast with this tendency; benzo[a]pyrene is the major component, and MW 252 PAHs predominate. PAHs with MW $\leqslant$ 202 partition between gas and particle phases (Kamens, Fulcher, & Guo, 1986). In this study, the aluminum foil collection substrate used is uncoated, preventing the onset of any positive adsorption artifact. It may be, for the studies being assessed, that gas-phase PAHs adsorb to quartz filter media or silicone impactor coatings, where appropriate, causing the trend of higher concentrations of lower MW particle-phase PAHs. An additional account is that a negative sampling artifact due to a relatively large sub-ambient pressure gradient ($\sim$ 10.0–38.7 kPa), which vaporizes the low MW PAH, at ELPI impactor stages 1–3 exists for our tests. However, low-pressure impactor stages sample PAH (MW $\geqslant$ 202) with vapor pressures less than 10^{-9} atm (298 K) with at least 98% efficiency (Venkataraman, Lyons, & Friedlander, 1994). Also, lower MW PAHs, due to their fast equilibration times and high flux, tend to associate with larger aerosols (Allen et al., 1998), which are collected near ambient pressures on the upper impactor stages (4–8). If valid, these arguments negate the negative sampling artifact as a probable cause of the considered trend. Further, the ultrafine ($d_a \leqslant 0.1$ μm) particles that the lower stages collect normally represent only a small fraction of the total particle mass. Other effects of MW and d_a on PAH equilibration are discussed.

4.4. PAH composition by particle size

Lognormal particle size distribution parameters (model-generated), d_g and σ_g of 24 individual PAHs (MW 202–302) in $PM_{2.5}$ emissions from RWC are shown (Table 4). For each source test, select PAH size distributions of emissions (μg/kg of dry biomass) are also given, Fig. 4. In our tests, the PAHs of wood smoke are unimodally distributed over accumulation and ultrafine particle size modes. Size distribution σ_g values are somewhat constant on an individual test basis, although PAHs in $PM_{2.5}$ of *Pseudotsuga* sp. are narrowly dispersed as indicated by their comparatively lower

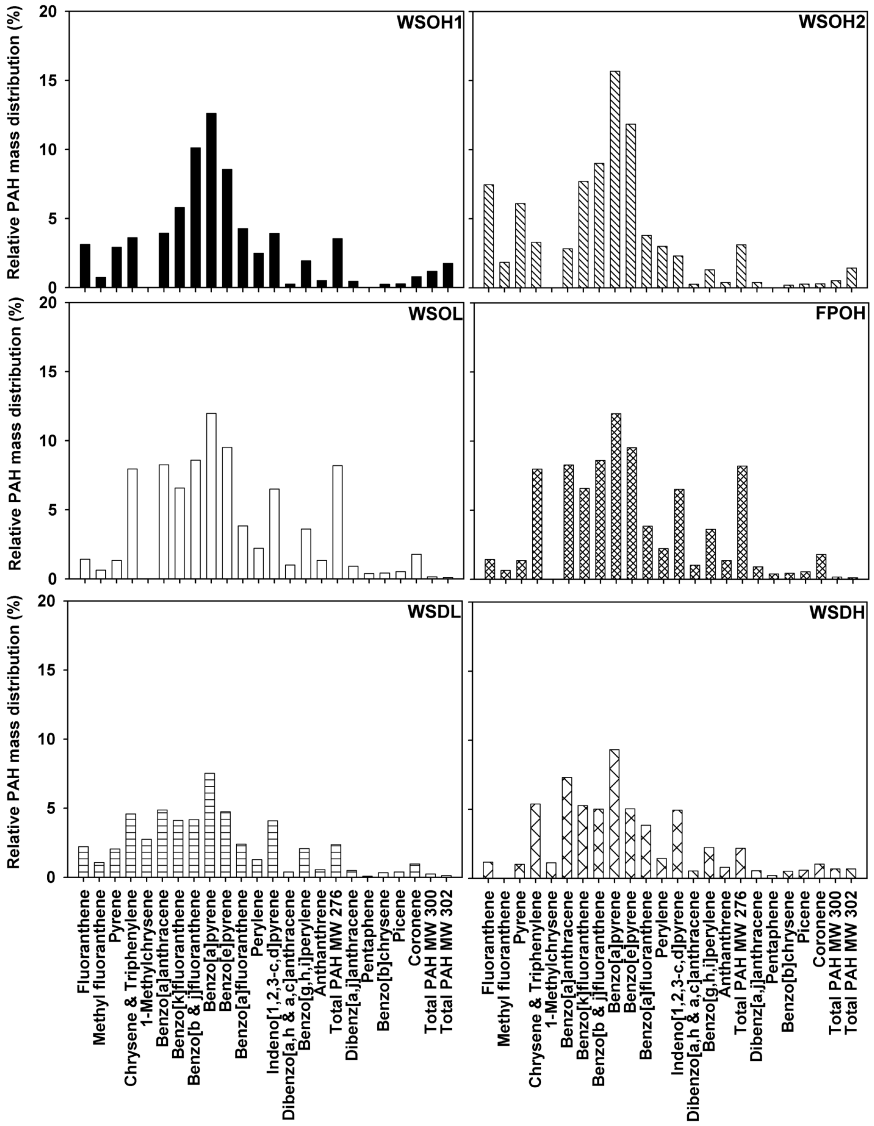

Fig. 3. Relative PAH mass distributions in $PM_{2.5}$ from RWC as determined by TD/GC/MS.

σ_g values. Compositional differences in biofuel, in effect, control emissions of pyrolysis products, but the exact dependence of σ_g (PAH) on biofuel type is uncertain and requires further testing.

Variations in combustion conditions across tests did not seem to modify PAH d_g values as a group. Figs. 2 and 4 show that the d_g range for PAH emissions is narrower than for $PM_{2.5}$ mass emissions. In addition to their narrower range, PAH size allocations are out of phase with $PM_{2.5}$ mass ones and consistently shifted to finer d_a. Clearly, the mechanisms that control formation of $PM_{2.5}$ and PAHs with respect to d_a are not entirely linked. Thermal breakdown and alteration of the cellulose polymer and steam-stripping distillation are among the particle formation mechanisms of

Table 4
Lognormal PAH-particle size distribution parameters (d_g and σ_g) modeled from TD/GC/MS-speciated and inverted ELPI stage data

Compound	Wood fuel type											
	Quercus sp./Oak								*Pseudotsuga* sp./Douglas fir			
	Log normal distribution parameters (geometric mean diameter [d_g, nm] and standard deviation [σ_g])											
	WSOH1		WSOH2		WSOL		FPOH		WSDL		WSDH	
	d_g	σ_g	d_g	σ_g	d_g	σ_g	d_g	σ_g	d_g	σ_g	d_g	σ_g
Fluoranthene	394	1.8	355	2.0			224	1.9	208	1.7	346	2.0
Pyrene	377	1.9	320	2.1			178	2.2	189	1.8	337	2.0
Acepyrene	349	1.5	294	1.9			202	1.2	175	1.4		
Methylchrysene									370	1.0		
Chrysene and Triphenylene	300	2.1	303	2.2			185	1.7	191	1.6	344	1.6
Benzo[*a*]anthracene	299	2.0	304	2.1			187	1.7	188	1.6	345	1.6
Benzo[*k*]fluoranthene	271	1.8	271	2.0	195	2.1	163	1.9	178	1.6	315	1.7
Benzo[$b + j$]fluoranthene	288	2.0	285	2.0	248	2.5	160	1.9	173	1.6	310	1.8
Benzo[*a*]pyrene	285	1.9	277	2.1	212	2.4	160	1.9	181	1.6	313	1.7
Benzo[*e*]pyrene	306	1.5	283	2.1	213	2.7	157	2.0	179	1.6	311	1.8
Benzo[*a*]fluoranthene	284	1.9	293	2.1	217	1.9	155	1.6	176	1.4	322	1.7
Perylene	359	1.6	279	1.5	199	2.0	153	1.7	177	1.4	310	1.8
Indeno[1, 2, 3-*cd*]pyrene	216	2.1	224	2.4	219	2.2	174	1.9	160	1.7	347	1.7
Dibenzo[$ah + ac$]anthracene			365	1.8	302	2.1	163	1.7	152	1.5	360	1.6
*n*Benzo[*ghi*]perylene	225	2.2	218	2.5	231	2.5	173	1.9	163	1.7	346	1.7
Anthanthrene	254	2.3	260	2.3	229	1.4	181	1.6	169	1.5	354	1.7
Total PAH MW 276	262	2.2	352	3.6	309	2.4	159	2.1	168	1.7	355	1.9
Dibenz[*aj*]anthracene	229	1.1	335	1.7	214	1.6	164	1.7	152	1.5	340	1.7
Pentaphene					263	1.2	168	1.7	164	1.3	361	1.5
Benzo[*b*]chrysene	337	1.4	352	1.8	285	1.3	162	1.7	200	1.4	351	1.6
Picene	340	1.4	331	1.7	235	1.1	165	1.7	186	1.4	366	1.6
Coronene	242	2.6	175	1.7	210	1.4	167	1.7	158	1.4	332	1.7
Total PAH MW 300	271	1.5	296	1.4	221	1.1	182	1.4	199	1.4	399	1.4
Total PAH MW 302	199	1.3	214	1.6	231	1.2	174	1.4	196	1.4	322	1.6

Notes: Range of r^2 values: WSOH1, 0.636–0.968; WSOH2, 0.741–0.988; WSOL, 0.447–0.992; FPOH, 0.744–0.993; WSDL, 0.806–0.987; WSDH, 0.923–0.985.

biomass combustion (Simoneit et al., 1999), while PAH growth is a multi-step process dependent on pyrolysis, progressive aromatization, and surface reaction yields (Violi et al., 1999). By MW class, largest margins of d_g offsets are 380 (WSOH1) and 363 nm (WSOH2) on average. For each test, this margin typically increases with PAH species MW. Within the PAH distribution, higher and lower MW PAH preferentially segregate to fine and coarse d_a, in that order as Fig. 5 supports. It appears that dilution in the wind tunnel used here adequately mimics atmospheric PAH equilibration because a similar pattern is noticed among atmospheric aerosol size fractions (Allen et al., 1996).

There are several explanations for this pattern: (a) PAH diffusivity inversely correlates with MW, affecting partitioning (Allen et al., 1996), (b) compared with smaller d_a particles, particles of larger

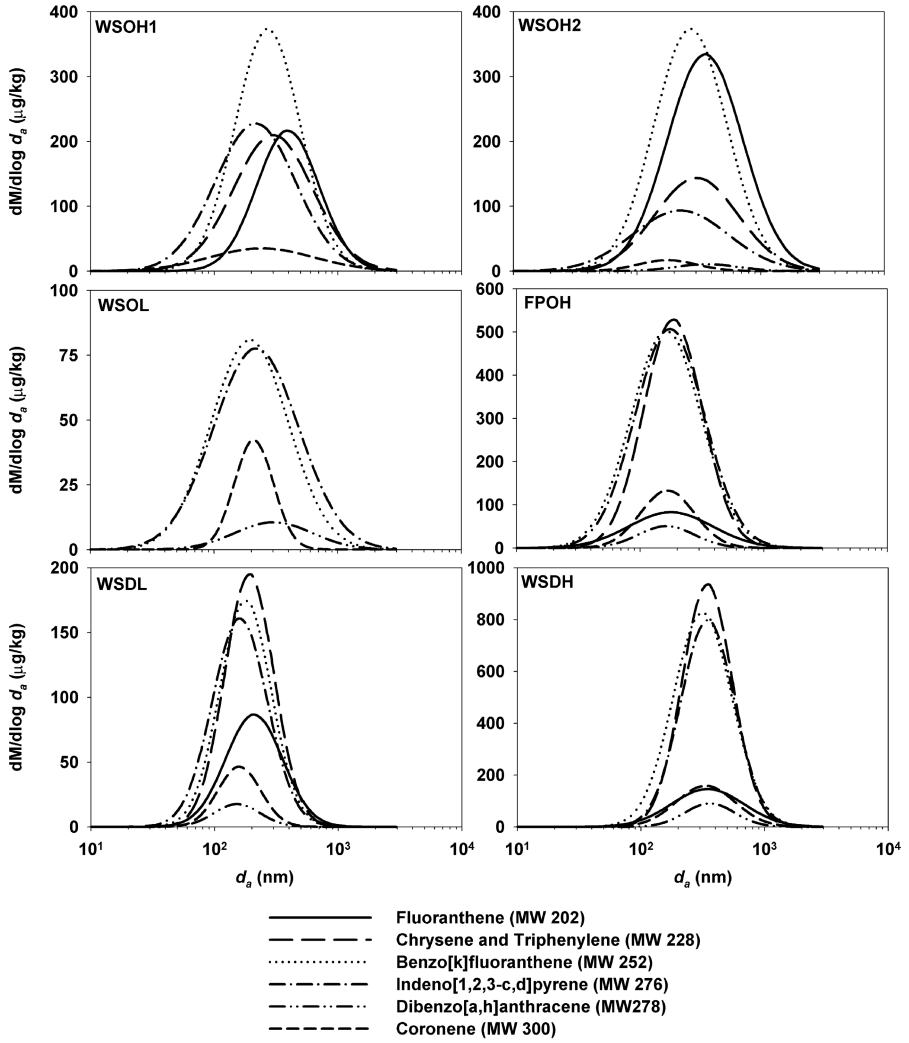

Fig. 4. Size distributions of select PAH compounds in $PM_{2.5}$ emissions from RWC.

d_a comprise more organic matter into which PAH are absorbed—wood smoke particles are primarily carbonaceous (Venkataraman, 2002), (c) curved surfaces of smaller particles produce higher partial pressures at equilibrium, which vaporizes volatile PAH that later condense onto larger particles (i.e. the Kelvin effect) (Venkataraman, Thomas, & Kulkarni, 1999; Zhang & Wexler, 2002), and (d) available surface areas change with d_a, effecting adsorption (Venkataraman et al., 1999 and references therein)—larger molecules align more easily over larger surface areas. We would also add that (1) in post-combustion cooling the pressure at which a condensate forms might be effected by particle pore size and structure and (2) resistance of interphase (gas → particle) mass transfer is reliant on surface and bulk chemical compositions, which demonstrate heterogeneity, comprise concentration gradients, and vary with d_a.

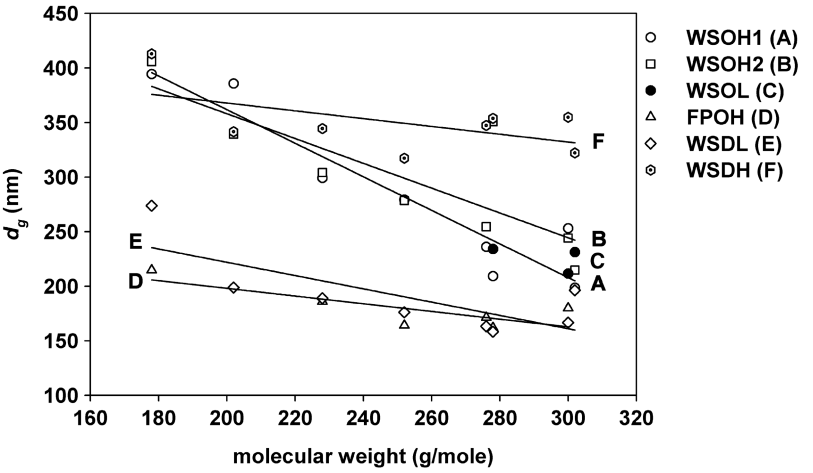

Fig. 5. Geometric mean diameters (d_g) of PAH from RWC by molecular weight class (MW).

Fig. 6 shows an accumulation of emission factors by MW and d_a for all PAH species and that the emissions of MW 252 PAH predominant. Attempts at modeling certain PAHs were unsuccessful (see Table 3), which explains why some data are omitted from the WSOL panel. Data of Fig. 6 confirm that particle PAH chemistry is unique to d_a, but obscure whether particles of identical d_a are externally mixed.

4.5. Adsorption versus absorption for particle-phase PAHs

Adsorption and absorption are the primary routes of PAH association with particles of small and large d_a, respectively. To examine the relationship between PM surface area and PAH concentrations, $dS/d\log d_a$ is plotted versus $dM/d\log d_a$ (the sum of all PAH) (Fig. 7). Values of $dS/d\log d_a$ are calculated from ELPI-determined particle number counts, the stage d_g, and by assuming sphericity. The ultrafine mode contains, on average, greater than 80% of the total measured particle number concentration and is measured down to 30 nm by ELPI. Values of d_g for particulate matter surface area range from 120–330 nm. For biomass combustion, PAH mass and PM surface area linearly correlate ($r^2 \geqslant 0.913$ for all tests, see Fig. 7). Likewise, PAH and surface area d_g values linearly correlate. However, formation of surface area is not categorically reliant on PAH growth. The negative y intercepts and inconsistent slopes in Fig. 7 support this observation. As discussed, other particle formation mechanisms are possible. For the WSDH test, the high PAH concentrations at low surface areas might indicate absorption. This judgment considers that, for the FPOH test, the surface area seems highly sensitive to PAH mass. Although, in reality, concluding much on adsorption and absorption with this approach is difficult.

The relationship derived by Venkataraman et al. (2002) indicates whether or not the particle surface composition comprises PAHs. In brief, $\log R = \log K - \log d_a$, where K is constant and $R =$ PAH mass/PM mass (using inverted data). In a plot of R versus d_a, a slope of -1 verifies that PAHs are associated with the particle surface. In this work, the PAH set is divided into seven molecular weight groups (202–302), Fig. 8. Results of the WSDL and FPOH tests (FPOH data are

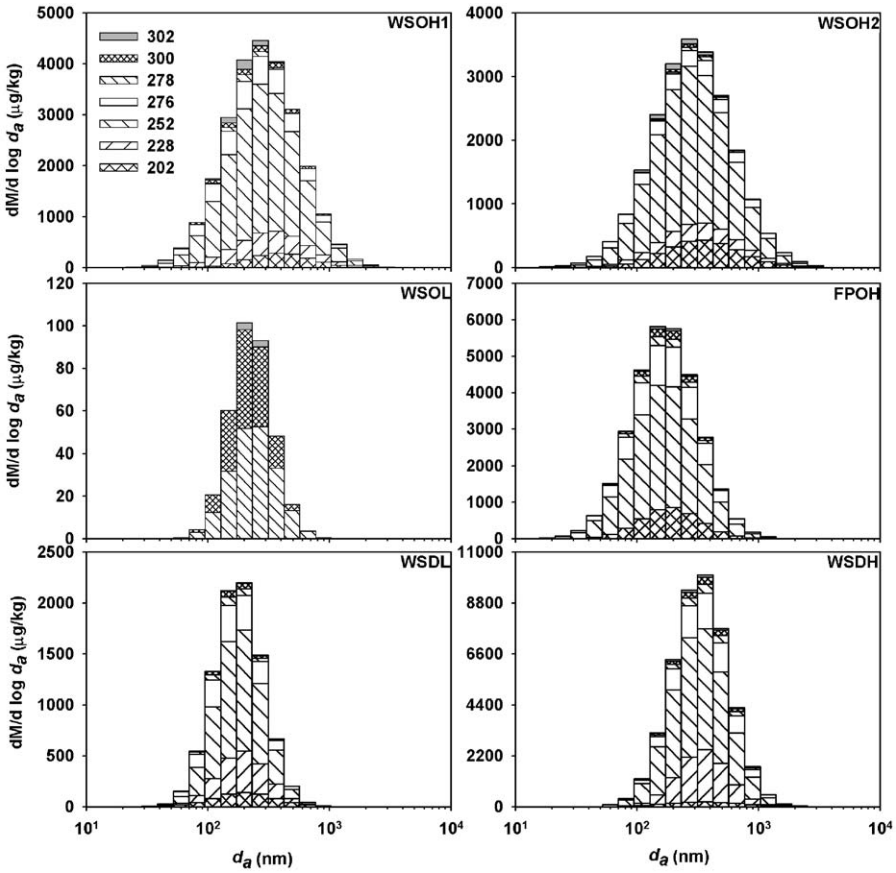

Fig. 6. Molecular weight-cumulative, PAH size distributions by combustion test.

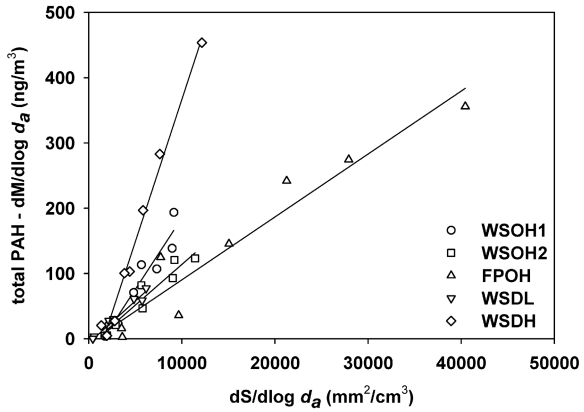

Fig. 7. Evidence of a linear relationship between PAH mass and calculated particle surface area values.

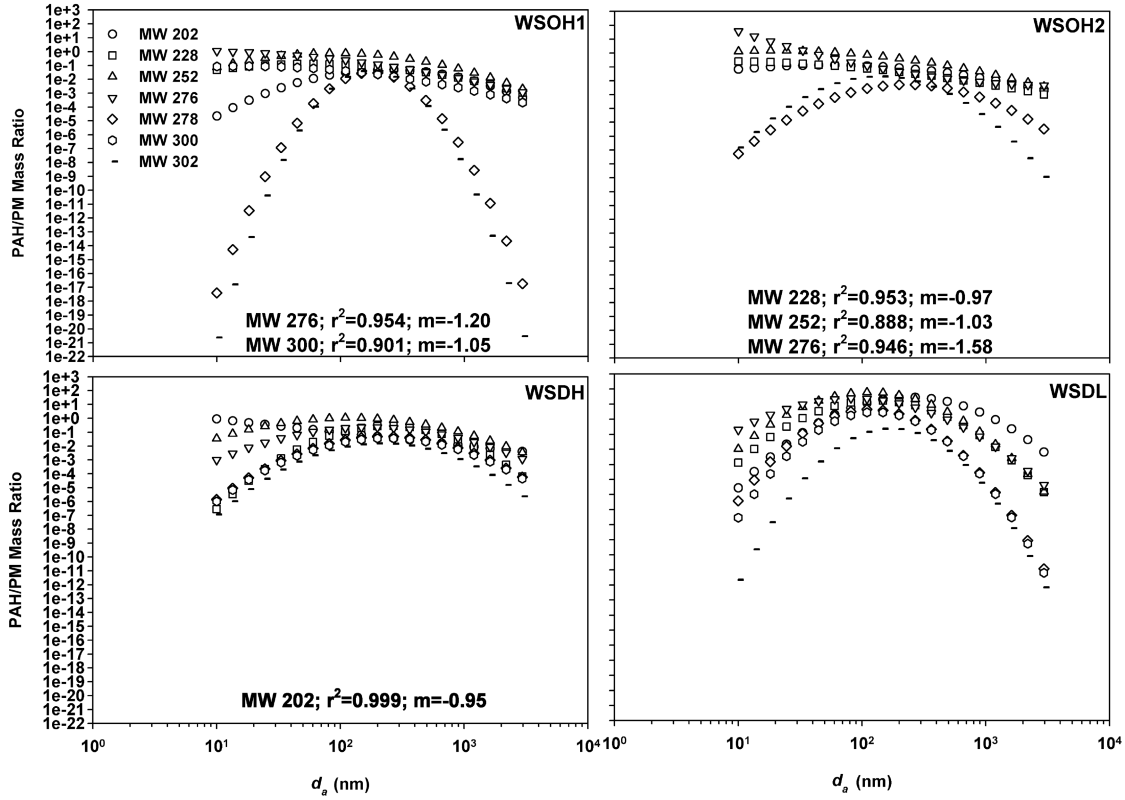

Fig. 8. Results of the data treatment used to obtain indication of the surface associations of PAH.

not shown but similar to those of WSDL) are inconclusive on an MW basis. An inconsistent trend for PAHs (lumped together) is also viewed for comparable biofuel combustion data (Venkataraman et al., 2002) and points to multiple mechanisms of PAH-particle associations, including absorption and adsorption.

For WSOH1 (MW 276, 300), WSOH2 (MW 228, 252, 276), and WSDH (MW 202), surface bound PAHs are evident as the slope ($m = -0.95$ to -1.58) and r^2 (0.888-0.999) values in the corresponding panels show. It is apparent that (a) particle surface and PAH core compositions of identical MW groups vary with combustion conditions, (b) preferential surface adsorption of lower MW PAH is possible, and (c) combustion aerosols of identical size from the same biomass fuel (WSOH1, WSOH2) likely comprise variable surface and core compositions of the same PAH. Physicochemical properties (such as water uptake, organic matter functionality, and morphology) of wood smoke particles, in effect, control the activity of the semivolatiles (Jang, Kamens, Leach, & Strommen, 1997; Jang & Kamens, 1998). Ionic composition of the particle(s) affects PAH adsorption (i.e., PAHs do not effectively co-desorb Ca and K) (Lazar, Reilly, Whitten, & Ramsey, 1999). We also expect that, for the combustion event, assorted fire regimes simultaneously burn different sections of the same fuel. This occurrence may randomly favor the emissions of certain compounds over others and, by varying compound concentration ratios, effect gas/particle equilibrium and particle formation.

Even so, the data treatment of Venkataraman et al. (2002) might be viewed as too simplistic because it assumes surface PAH and particle densities stay consistent with d_a (Venkataraman, 2002).

Individual PAHs may be conserved under ambient conditions and implemented as molecular markers in source apportionment calculations (Schauer, Rogge, Hildemann, Mazurek, & Cass, 1996; Fraser, Kleeman, Schauer, & Cass, 2000). Air quality model predictions now track PM source emissions using air parcels polluted with size distributed chemical mixtures (Bhave et al., 2002 and references therein). PAH size distributions and concentrations can vary with respect to source type. Evidence of this effect is offered by comparing RWC emissions with those of traffic tunnel studies (Venkataraman et al., 1994; Miquel, Kirchstetter, Harley, & Hering, 1998). Gasoline- and diesel-powered vehicles in tunnel traffic emit predominantly ultrafines, which are uniquely dispersed against the accumulation mode particles that also result. Of course, RWC aerosols are primarily accumulation mode; source-oriented, mixed compositions in ambient aerosols of the same size are possible (Kleeman, Cass, & Eldering, 1997). This stresses the importance of the relative concentrations of PAH in aerosol emissions, which, due to vehicle and fuel types and probably operating conditions, vary profoundly with MW. Because individual wood combustion and mobile source PAHs are emitted at variable concentrations, rates, and size mode intervals, their eventual use in apportionment work is expected. Additional size segregation work by source is forthcoming.

The toxic properties of PAHs are well documented (Schoey, 1998; Vinggaard et al., 2000). Fine PM from RWC is linked to adverse health impacts (Larson & Koenig, 1994; Pintos et al., 1998). Considering the PAH in wood smoke associate with particles over ultrafine and accumulation modes, they putatively deposit in nasopharyngeal, tracheo-bronchial, and pulmonary zones of the respiratory tract. With higher MW PAH spread over smaller d_a, the probability of them depositing in the deep lung is increased. In the final analysis, the apparent variation in surface composition of the PAH MW groups (for the same source) is expected to even further complicate the emergence of a single mechanism to describe the negative health impacts linked to fine particulate matter from wood combustion.

References

Allen, J. O., Dookeran, N. M., Smith, K. A., Sarofim, A. F., Taghizadeh, K., & Lafleur, A. L. (1996). Measurement of polycyclic aromatic hydrocarbons associated with size-segregated atmospheric aerosols in Massachusetts. *Environmental Science and Technology*, *30*, 1023–1031.

Allen, J. O., Dookeran, N. M., Taghizadeh, K., Lafleur, A. L., Smith, K. A., & Sarofim, A. F. (1997). Measurement of oxygenated polycyclic aromatic hydrocarbons associated with a size-segregated urban aerosol. *Environmental Science and Technology*, *31*, 2064–2070.

Allen, J. O., Durant, J. L., Dookeran, N. M., Taghizadeh, K., Plummer, E. F., Lafleur, A. L., Sarofim, A. F., & Smith, K. A. (1998). Measurement of $C_{24}H_{14}$ polycyclic aromatic hydrocarbons associated with a size-segregated urban aerosol. *Environmental Science and Technology*, *32*, 1928–1932.

Balashazy, I., Hofmann, W., & Heistracher, T. (1999). Computation of local enhancement factors for the quantification of particle deposition patterns in airway bifurcations. *Journal of Aerosol Science*, *30*, 185–203.

Bhave, P. V., Kleeman, M. J., Allen, J. O., Hughes, L. S., Prather, K. A., & Cass, G. R. (2002). Evaluation of an air quality model for the size and composition of source-oriented particle classes. *Environmental Science and Technology*, *36*, 2154–2163.

Diociaiuti, M., Balduzzi, M., De Berardis, B., Cattani, G., Stacchini, G., Ziemacki, G., Marconi, A., & Paoletti, L. (2001). The two PM(2.5)(fine) and PM(2.5-10)(coarse) fractions: Evidence of different biological activity. *Environmental Research*, *86*, 254–262.

Dockery, D. W., Pope, A. C., Xu, X., Spengler, J. D., Ware, J. H., Fay, M. E., Ferris Jr., B. G., & Speizer, F. E. (1993). An association between air pollution and mortality in six U.S. Cities. *The New England Journal of Medicine*, *393*, 1753–1759.

Falkovich, A. H., & Rudich, Y. (2001). Analysis of semivolatile organic compounds in atmospheric aerosols by direct sample introduction thermal desorption GC/MS. *Environmental Science and Technology*, *35*, 2326–2333.

Fine, P. M., Cass, G. R., & Simoneit, B. R. T. (2001). Chemical characterization of fine particle emissions from fireplace combustion of woods grown in the northeastern United States. *Environmental Science and Technology*, *35*, 2665–2675.

Fraser, M. P., Kleeman, M. J., Schauer, J. J., & Cass, G. R. (2000). Modeling the atmospheric concentrations of individual gas-phase and particle-phase organic compounds. *Environmental Science and Technology*, *34*, 1302–1312.

Gullett, B. K., Touati, A., & Hays, M. D. (2003). PCDD/F, PCB, HxCBz, PAH and PM emission factors for fireplace and woodstove combustion in the San Francisco Bay region. *Environmental Science and Technology*, *37*, 1758–1765.

Hauser, R., Godleski, J. J., Hatch, V., & Christiani, D. C. (2001). Ultrafine particles in human lung macrophages. *Archives of Environmental Health*, *56*, 150–156.

Hays, M. D., Geron, C. D., Linna, K. J., Smith, N. D., & Schauer, J. J. (2002). Speciation of gas-phase and fine particle emissions from burning of foliar fuels. *Environmental Science and Technology*, *36*, 2281–2295.

Jang, M., & Kamens, R. M. (1998). A thermodynamic approach for modeling partitioning of semivolatile organic compounds on atmospheric particulate matter: Humidity effects. *Environmental Science and Technology*, *32*, 1237–1243.

Jang, M., Kamens, R. M., Leach, K. B., & Strommen, M. R. (1997). A thermodynamic approach using group contribution methods to model the partitioning of semivolatile organic compounds on atmospheric particulate matter. *Environmental Science and Technology*, *31*, 2805–2811.

Kamens, R. M., Fulcher, J. N., & Guo, Z. (1986). Effects of temperature on wood soot PAH decay in atmospheres with sunlight and low NO_x. *Atmospheric Environment*, *20*, 1579–1587.

Keskinen, J., Pietarinen, K., & Lehtimaki, M. (1992). Electrical low pressure impactor. *Journal of Aerosol Science*, *23*, 353–360.

Kleeman, M. J., Cass, G. R., & Eldering, A. (1997). Modeling the airborne particle complex as a source-oriented external mixture. *Journal of Geophysical Research*, *102*, 21355–21372.

Kleeman, M. J., Schauer, J. J., & Cass, G. R. (1999). Size and composition distribution of fine particulate matter emitted from wood burning, meat charbroiling, and cigarettes. *Environmental Science and Technology*, *33*, 3516–3523.

Kleeman, M. J., Schauer, J. J., & Cass, G. R. (2000). Size and composition distribution of fine particle matter emitted from motor vehicles. *Environmental Science and Technology*, *34*, 1132–1142.

Larson, T. V., & Koenig, J. Q. (1994). Wood smoke: Emissions and noncancer respiratory effects. *Annual Review of Public Health*, *15*, 133–156.

Lazar, A. C., Reilly, P. T. A., Whitten, W. B., & Ramsey, J. M. (1999). Real-time surface analysis of individual airborne environmental particles. *Environmental Science and Technology*, *33*, 3993–4001.

Marjamaki, M., Keskinen, J., Chen, D. -R., & Pui, D. Y. H. (2000). Performance evaluation of the electrical low-pressure impactor (ELPI). *Journal of Aerosol Science*, *31*, 249–261.

McDonald, J. D., Zielinska, B., Fujita, E. M., Sagebiel, J. C., Chow, J. C., & Watson, J. G. (2000). Fine particle and gaseous emission rates from residential wood combustion. *Environmental Science and Technology*, *34*, 2080–2091.

McDonald, J. D., Zielinska, B., Sagebiel, J. C., & McDaniel, M. R. (2002). Characterization of fine particle matter in ambient air and personal samples from an underground mine. *Aerosol Science and Technology*, *36*, 1033–1044.

Miquel, A. H., Kirchstetter, T. W., Harley, R. A., & Hering, S. V. (1998). On-road emissions of particulate polycyclic aromatic hydrocarbons and black carbon from gasoline and diesel vehicles. *Environmental Science and Technology*, *32*, 450–455.

Moisio, M., Hautanen, J., Virtanen, A., Marjamaki, M., & Keskinen, J. (1997). Electrical low pressure impactor data processing-effect of particle density. *Journal of Aerosol Science*, *28*, S143–S144.

Nolte, C. G., Schauer, J. J., Cass, G. R., & Simoneit, B. R. T. (2001). Highly polar organic compounds present in wood smoke and in the ambient atmosphere. *Environmental Science and Technology*, *35*, 1912–1919.

Oanh, N. T. K., Nghiem, L. H., & Phyu, Y. L. (2002). Emission of polycyclic aromatic hydrocarbons, toxicity, and mutagenicity from domestic cooking using sawdust briquettes, wood, and kerosene. *Environmental Science and Technology*, *36*, 833–839.

Oberdörster, G. (2001). Pulmonary effects of inhaled ultrafine particles. *International Archives of Occupational and Environmental Health*, *74*, 1–8.

Offenberg, J. H., & Baker, J. E. (1999). Aerosol size distributions of polycyclic aromatic hydrocarbons in urban and over-water atmospheres. *Environmental Science and Technology*, *33*, 3324–3331.

Phalen, R. F., Cuddihy, R. G., Fisher, G. L., Moss, O. R., Schlesinger, R. B., Swift, D. L., & Yeh, H. C. (1991). Main features of the proposed NCRP respiratory tract model. *Radiation Protection Dosimetry*, *38*, 179–184.

Pintos, J., Franco, E. L., Kowalski, L. P., Oliveira, B. V., & Curado, M. P. (1998). Use of wood stoves and risk of cancers of the upper aero-digestive tract: A case-control study. *International Journal of Epidemiology*, *27*, 936–940.

Pope, C. A. (2000). Epidemiology of fine particulate air pollution and human health: Biologic mechanisms and who's at risk?. *Environmental Health Perspectives*, *108*, 713–723.

Purvis, C. R., McCrillis, R. C., & Kariher, P. H. (2000). Fine particulate matter (PM) and organic speciation of fireplace emissions. *Environmental Science and Technology*, *34*, 1653–1658.

Rogge, W. F., Hildemann, L. M., Mazurek, M. A., & Cass, G. R. (1998). Sources of fine organic aerosol. 9. Pine oak, and synthetic log combustion in residential fireplaces. *Environmental Science and Technology*, *32*, 13–22.

Samet, J. M., Dominici, F., Curriero, F. C., Coursac, I., & Zeger, S. L. (2000). Fine particulate air pollution and mortality in 20 U.S. cities, 1987–1994. *The New England Journal of Medicine*, *343*, 1742–1749.

Sanders, L. C., & Wise, S. A. *Polycyclic aromatic hydrocarbon structure index*. http://ois.nist.gov/pah/ (accessed January 6, 2002).

Schauer, J. J., Kleeman, M. J., Cass, G. R., & Simoneit, B. R. T. (2001). Measurement of emissions from air pollution sources. 3. C1-C29 organic compounds from fireplace combustion of wood. *Environmental Science and Technology*, *35*, 1716–1728.

Schauer, J. J., Rogge, W. F., Hildemann, L. M., Mazurek, M. A., & Cass, G. R. (1996). Source apportionment of airborne particulate matter using organic compounds as tracers. *Atmospheric Environment*, *30*, 3837–3855.

Schoey, R. (1998). Human health risk assessment of environmental mixtures of polycyclic aromatic hydrocarbons (PAH). *Pathophysiology*, *5*, 111.

Silva, P. J., Liu, D., Noble, C. A., & Prather, K. A. (1999). Size and chemical characterization of individual particles resulting from biomass burning of local southern California species. *Environmental Science and Technology*, *33*, 3068–3076.

Silva, P. J., & Prather, K. A. (1997). On-line characterization of individual particles from automobile emissions. *Environmental Science and Technology*, *31*, 3074–3080.

Simoneit, B. R. T., Schauer, J. J., Nolte, C. G., Oros, D. R., Elias, V. O., Fraser, M. P., Rogge, W. F., & Cass, G. R. (1999). Levoglucosan, a tracer for cellulose in biomass burning and atmospheric particles. *Atmospheric Environment*, *33*, 173–182.

Swift, D. L. (1995). The oronasal airways: The definer and ignored respiratory zone of PM-10 regulatory convention. *Inhalation Toxicology*, *7*, 125–130.

Tobias, H. J., & Ziemann, P. J. (1999). Compound identification in organic aerosols using temperature-programmed thermal desorption particle beam mass spectrometry. *Analytical Chemistry*, *71*, 3428–3435.

Tobias, H. J., Beving, D. E., Ziemann, P. J., Sakurai, H., Zuk, M., McMurry, P. H., Zarling, D., Waytulonis, R., & Kittelson, D. B. (2001). Chemical analysis of diesel engine nanoparticles using a nano-DMA/thermal desorption particle beam mass spectrometer. *Environmental Science and Technology*, *35*, 2233–2243.

Tsuda, A., Rogers, R. A., Hydon, P. E., & Butler, J. P. (2002). Chaotic mixing deep in the lung. *Proceedings of the National Academy of Sciences*, *99*, 10173–10178.

U.S. EPA. (2001). Office of Air Quality Planning and Standards: Clearinghouse for emission inventories and emission factors. http://www.epa.gov/ttn/chief/index.html (accessed May 2001).

Venkataraman, C. (2002). On PAH size distributions, *personal communication*.

Venkataraman, C., Lyons, J. M., & Friedlander, S. K. (1994). Size distributions of polycyclic aromatic hydrocarbons and elemental carbon. 1. Sampling, measurement methods, and source characterization. *Environmental Science and Technology*, *28*, 555–562.

Venkataraman, C., Negi, G., Sardar, S. B., & Rastogi, R. (2002). Size distributions of polycyclic aromatic hydrocarbons in aerosol emissions from biofuel combustion. *Journal of Aerosol Science*, *33*, 503–518.

Venkataraman, C., & Rao, G. U. M. (2001). Emission factors of carbon monoxide and size-resolved aerosols from biofuel combustion. *Environmental Science and Technology*, *35*, 2100–2107.

Venkataraman, C., Thomas, S., & Kulkarni, P. (1999). Size distributions of polycyclic aromatic hydrocarbons-gas/particle partitioning to urban aerosols. *Journal of Aerosol Science*, *30*, 759–770.

Vinggaard, A. M., Hnida, C., & Larsen, J. C. (2000). Environmental polycyclicaromatic hydrocarbons affect androgen receptor activation in vitro. *Toxicology*, *145*, 173–183.

Violi, A., D'Anna, A., & D'Alessio, A. (1999). Modeling of particulate formation in combustion and pyrolysis. *Chemical Engineering Science*, *54*, 3433–3442.

Virtanen, A., Marjamaki, M., Ristimaki, J., & Keskinen, J. (2001). Fine particle losses in electrical low-pressure impactor. *Journal of Aerosol Science*, *32*, 389–401.

Waterman, D., Horsfield, B., Leistner, F., Hall, K., & Smith, S. (2000). Quantification of polycyclic aromatic hydrocarbons in the NIST standard reference material (SRM 1649a) urban dust using thermal desorption GC/MS. *Analytical Chemistry*, *72*, 3563–3567.

Winklmayr, W., Wang, H.-C., & John, W. (1990). Adaptation of the Twomey algorithm to the inversion of cascade impactor data. *Aerosol Science and Technology*, *13*, 322–331.

Wise, S. A., Sander, L. C., Schantz, M. M., Hays, M. J., & Benner Jr., B. A. (2000). Recertification of standard reference material (SRM) 1649, urban dust, for the determination of polycyclic aromatic hydrocarbons (PAHs). *Polycyclic Aromatic Compounds*, *13*, 419–456.

Zhang, K. M., & Wexler, A. S. (2002). Modeling the number distributions of urban and regional aerosols: Theoretical foundations. *Atmospheric Environment*, *36*, 1863–1874.